Wang, T., Zhuang, J., Buckby, J., Obara, K., Tsuruoka, H. (2018) JGR, 123, 6802-6825. https://doi.org/10.1029/2017JB015360

Identifying the recurrence patterns of non-volcanic tremors using a 2D hidden Markov model with extra zeros

Ting Wang[1], Jiancang Zhuang[2,3,4], Jodie Buckby[1], Kazushige Obara[5], and Hiroshi Tsuruoka[5]

[1]Department of Mathematics and Statistics, University of Otago, Dunedin, New Zealand
[2]Institute of Statistical Mathematics, Tokyo, Japan
[3]Department of Statistical Science, the Graduate University for Advanced Studies, Tokyo, Japan
[4]London Mathematical Laboratory
[5]Earthquake Research Institute, University of Tokyo, Tokyo, Japan

Key Points:

- A 2D hidden Markov model is proposed for automated and robust classification of tremor swarms
- We identify a hierarchical structure with three types of tremor quantitatively classified and provide clear boundaries between tremor swarms
- We provide probabilistic forecasts of tremor activity

Abstract

Non-volcanic tremor activity has been observed in many places worldwide. In some regions, their activity was observed to accompany slow slip events. Before examining whether and how non-volcanic tremor activity is related to slow slip, it is essential to understand quantitatively the spatiotemporal migration patterns of non-volcanic tremors. We developed a 2D hidden Markov model to automatically analyze and forecast the spatiotemporal behaviour of tremor activity in the regions Kii and Shikoku, southwest Japan. This new automated procedure classifies the tremor source regions into distinct segments in 2D space and infers a clear hierarchical structure of tremor activity, where each region consists of several subsystems and each subsystem contains several segments. The segments can be quantitatively categorized into three different types according to their occurrence patterns: episodic, weak concentration, and background, extending earlier knowledge gained from hand-picked tremor swarms. The Kii region can be categorized into four different subsystems, with two often linked to each other. The Shikoku region can be divided into six subsystems, with two in central Shikoku linked to each other. Moreover, a significant increase in the proportion of tremor occurrence was detected in a segment in southwest Shikoku before the 2003 and 2010 long-term slow slip events in the Bungo channel. This highlights the possible correlation between non-volcanic tremor and slow slip events. The model can be used to analyze tremor data from other regions.

1 Introduction

Both slow slip and earthquakes release accumulated strain due to tectonic movements. It is generally difficult to detect the onset of a slow slip event prospectively. Repeated slow slip events have been observed to be accompanied by non-volcanic tremors [e.g., *Rogers and Dragert*, 2003; *Obara et al.*, 2010; *Hirose and Obara*, 2010;

Corresponding author: Ting Wang, ting.wang@otago.ac.nz

Obara, 2011]. If a relationship between non-volcanic tremor events and slow slip events could be established, then the spatiotemporal patterns of non-volcanic tremors could provide a probabilistic forecast of slow slip events.

There are short-term and long-term slow slip events. Short-term slow slip events are collocated with tremor episodes in space and time, and usually last for days [*Obara and Kato*, 2016]. Long-term slow slip events are normally located at the up-dip side of tremor source regions and last for months to years [*Obara and Kato*, 2016]. Several studies reported the observation of crustal deformation caused by short-term slow slip events during the occurrence of tremor in the Cascadia and Nankai subduction zones [e.g., *Rogers and Dragert*, 2003; *Obara et al.*, 2004; *Hirose and Obara*, 2010; *Obara*, 2011]. Following the onset of the long-term slow slip events in south central Alaska, *Peterson and Christensen* [2009] found many occurrences of non-volcanic tremors in the region.

Not all tremor occurrences are associated with long-term or short-term slow slip events. Identifying which spatial segments are associated with slow slip events and how frequently this association recurs will help us understand more about their geophysical relationship. To examine how they are related to each other, it is crucial to classify and investigate the spatial and temporal migration patterns of the well recorded tremors quantitatively. *Brudzinski and Allen* [2007] and *Holtkamp and Brudzinski* [2010] divided the Cascadia tremor sources into along-strike spatial segments and studied their recurrence intervals. Since then, recurrence patterns along-dip and/or along-slip have been described for the Cascadia subduction zone [*Wech and Creager*, 2011; *Boyarko et al.*, 2015] and the Nankai subduction zone [*Obara et al.*, 2012].

Currently, the identification of spatial segments of tremor activity is done manually. With technological advances in observational instruments and the increased quantity of observed non-volcanic tremors worldwide, there is a need to develop some statistical tools to analyze the spatiotemporal migration pattern of tremor sources systematically. An automated quantitative approach could provide fast classification of tremors and identify features in the data overlooked by qualitative methods. Additionally, subsets of data which might be of interest can be extracted and analyzed with ease for more comprehensive understanding of migration patterns. Then the relationship between slow slip and tremor can be better understood.

Wang et al. [2016] developed a 1D hidden Markov model (HMM) to investigate the spatiotemporal migration pattern of tremor clusters in the Tokai region in Japan. They projected the 2D spatial locations onto a line to reduce the dimension, which worked well for the tremors in the Tokai region as the locations can be well approximated by 1D projection and there were not many observations available. However, tremor events in some regions have more complicated clustering structure in space which cannot be explained by a 1D projection [*Obara*, 2010, 2011]. In this paper, we propose to use a 2D HMM to analyze the spatiotemporal migration of tremors in the Kii and Shikoku regions. We also detect further temporal patterns of each spatial segment identified by the HMM model and use this model to carry out probabilistic forecasts of tremor activity in the two regions.

2 Data

There are three major regions in which active non-volcanic tremor occurrences have been detected in and near the Nankai subduction zone: the Tokai, Kii, and Shikoku regions. Tremor activity spans along the strike of the Philippine Sea Plate for about 600km, and the depth ranges from 30km to 45km on the plate interface [*Obara et al.*, 2012]. Along-strike and slip-parallel migrations of tremor activity in the Kii region have been described in *Obara et al.* [2012].

Non-volcanic tremor was first detected in the Nankai subduction zone in Japan by *Obara* [2002]. Since then, new methods have been proposed to improve the location and detection of non-volcanic tremors [e.g., *Kao and Shan*, 2004; *Shelly et al.*, 2006; *Maeda and Obara*, 2009]. We use the hourly centroid catalog from 2001 to 2012 determined using a clustering method as described in *Obara et al.* [2010]. The centroid locations of tremors in each hour are derived from the tremor locations obtained in 1-minute intervals using the modified envelop correlation method [*Maeda and Obara*, 2009]. The original waveform data is from the High Sensitivity Seismograph Network of the National Research Institute for Earth Science and Disaster Prevention in Japan. Figure 1 shows the non-volcanic tremors in the Kii and Shikoku regions from January 2001 to December 2012. Tremor occurs sporadically in segments of both space and time which can be clearly seen in Figure 4.

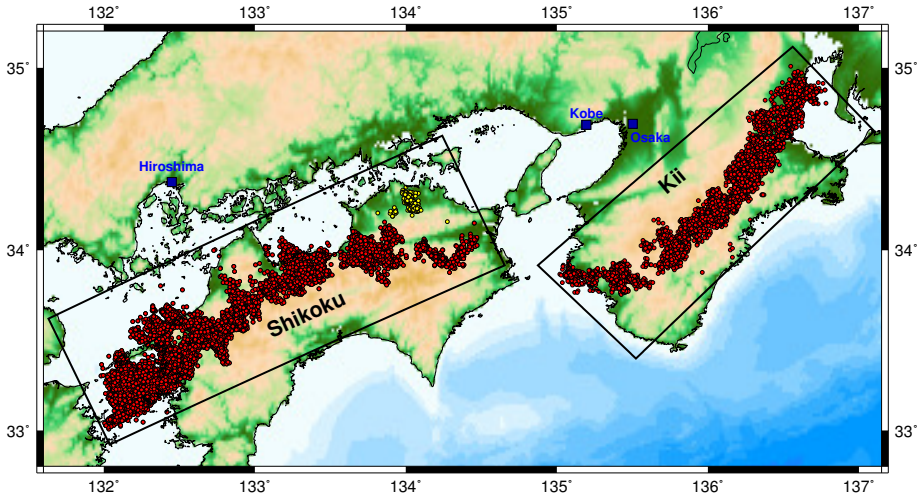

Figure 1. The locations of tremors in the Kii and Shikoku region.

3 Methodology

HMMs have wide applications, and have recently been applied in earth sciences such as modeling GPS measurement of ground deformation [*Granat and Donnellan*, 2002; *Wang and Bebbington*, 2013], seismic activity [*Orfanogiannaki et al.*, 2010; *Wang et al.*, 2012], and volcanic activity [*Bebbington*, 2007]. For a comprehensive introduction, please refer to *MacDonald and Zucchini* [1997].

An HMM is a statistical model in which the observed process is dependent on an unobserved Markov chain. A Markov chain is a sequence of states which exhibits a short-memory property such that the current state of the chain is dependent only on the previous state in the case of a first-order Markov chain. Given the previous state, the current state is independent of any state prior to that. An HMM is often used for time series data, in which the observed data can be classified into different groups over time. The unobserved Markov chain describes the number of distinct groups in the data and the transition pattern over time between each pair of groups. The aim of using such a model is to use the observed time series data to estimate the most likely Markov chain and thus provide the most likely classification of the time series data.

Figure 2 illustrates the structure of an HMM. Assume that the Markov chain has m states, where m can be estimated from the data. Let $S_t \in \{1, \cdots, m\}$ denote the state of the Markov chain at time t. The probability of a first-order Markov chain

in state j at time t given the previous states is $P(S_t = j \mid S_{t-1}, \cdots, S_1) = P(S_t = j \mid S_{t-1})$. These states are not observable. The observation Y_t at time t depends on the state S_t of the Markov chain. In this framework, we are interested in estimating the transition probability matrix $\mathbf{\Gamma} = (\gamma_{ij})_{m\times m}$ of the Markov chain that describes the migration pattern and the density function $f(y_t|S_t = i)$ that gives the distribution feature of observations in state i, where $\gamma_{ij} = P(S_t = j \mid S_{t-1} = i)$. For a stationary Markov chain, $\boldsymbol{\pi}\mathbf{\Gamma} = \boldsymbol{\pi}$, where $\boldsymbol{\pi} = (\pi_1, \pi_2, \cdots, \pi_m)$ is the row vector of the stationary probabilities for the m states. After the system enters a specific state i, the time that it stays in this state is called the sojourn time in state i.

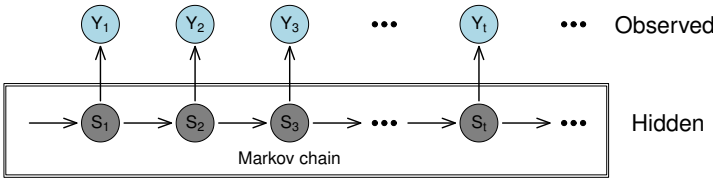

Figure 2. A diagram for the structure of an HMM.

As shown in *Wang et al.* [2016], an HMM is a useful tool to identify the centers of spatial segments of tremor activity and quantify the migration pattern among the segments. In their model, each unobserved state represents a distinct spatial segment, and the transition between different states describes the migration of tremor activity between different segments. The observed data at each time point consist of an indication of whether or not tremor occurred at that time point, and if so the location of tremor.

If we take a short period of time in the space-time plot, we see another feature in the data. There is no tremor observed at most times, so we have many null events in the time series. Following the previous work of *Wang et al.* [2016], the tremor data can be considered as being generated from a system with two components: one is binary and indicates whether a tremor cluster is present or not at time t; and the other describes where the tremor cluster locates conditional on the presence of a tremor cluster at time t. We can use a Bernoulli variable to model whether or not tremor occurs, and then use a continuous multivariate distribution to model the location of the tremor cluster when it occurs.

Let Z_t be a Bernoulli variable with

$$Z_t = \begin{cases} 1, & \text{a tremor cluster is present at } t \\ 0, & \text{otherwise} \end{cases}$$

Let $\mathbf{X}_t$ be the location of the tremor cluster in two-dimensional space at time t. From *Wang et al.* [2016] we can see that the tremor activity aggregates into several segments in space. If we consider the segments separately, then the tremor location $\mathbf{X}_t$ in each segment has a distribution with distinct central location (mean) and spread (variance). The tremor activity migrates among these segments. Each segment is considered as a state of the Markov chain S_t at time t, with state space $\{1, \cdots, m\}$.

The observational space of the entire system is $\{0\} \cup \big(\{1\}\times\mathbf{R}^2\big)$, where $\mathbf{R}^2$ denotes the two-dimensional vector space of real numbers. The probabilities that the observation falls in $\{0\}$ and $\{1\}\times\mathbf{R}^2$ when the system is in state i at time t are $1 - p_i$ and p_i respectively, i.e., $P(Z_t = 0 \mid S_t = i) = 1 - p_i$ and $P(Z_t = 1 \mid S_t = i) = p_i$. We assume that, given $Z_t = 1$ and $S_t = i$, $\mathbf{X}_t$ follows a multivariate normal distribution, i.e.,

$$f(\mathbf{x}_t \mid Z_t = 1, S_t = i) = \frac{1}{2\pi|\mathbf{\Sigma}_i|^{1/2}} \exp\left(-\frac{1}{2}(\mathbf{x}_t - \boldsymbol{\mu}_i)^T \mathbf{\Sigma}_i^{-1}(\mathbf{x}_t - \boldsymbol{\mu}_i)\right).$$

The joint probability density function of Z_t and $\mathbf{X}_t$ conditional on the system being in state i at time t is

$$f(\mathbf{x}_t, z_t \mid S_t = i) = (1-p_i)^{1-z_t}\left[p_i \frac{1}{2\pi|\mathbf{\Sigma}_i|^{1/2}} \exp\left(-\frac{1}{2}(\mathbf{x}_t-\boldsymbol{\mu}_i)^T\mathbf{\Sigma}_i^{-1}(\mathbf{x}_t-\boldsymbol{\mu}_i)\right)\right]^{z_t}, \quad (1)$$

where p_i, $\boldsymbol{\mu}_i = E(\mathbf{X}_t|S_t = i, Z_t = 1)$ and $\mathbf{\Sigma}_i = Var(\mathbf{X}_t|S_t = i, Z_t = 1)$ are parameters to be estimated.

The parameters that need to be estimated from the observed data are: the transition probability matrix $\mathbf{\Gamma} = (\gamma_{ij})_{m\times m}$ of the Markov chain that describes the migration pattern, where $\gamma_{ij} = P(S_t = j \mid S_{t-1} = i)$; the row vector of the stationary probabilities for the m states, $\boldsymbol{\pi} = (\pi_1, \pi_2, \cdots, \pi_m)$; the probability of tremor occurrence when the system is in state i at time t, $p_i = P(Z_t = 1 \mid S_t = i)$; mean $\boldsymbol{\mu}_i = E(\mathbf{X}_t|S_t = i, Z_t = 1)$ and variance $\mathbf{\Sigma}_i = Var(\mathbf{X}_t|S_t = i, Z_t = 1)$ of tremor events in each state.

Given the number of states for the model, the model parameters can be estimated by using the Expectation-Maximization (EM) algorithm [*Baum et al.*, 1970; *Dempster et al.*, 1977]. The details of the EM algorithm are in Appendix A. To determine the number of states, we first fit HMMs with different numbers of states to the data, and then use the Bayesian Information Criterion [BIC, *Schwarz*, 1978] to compare these models. The BIC is defined as BIC $= -2\log(\text{likelihood}) + k\log(T)$, where k is the number of parameters to be estimated and T is the number of observations. The model with the smallest BIC value is chosen as the optimal one among the candidate models.

After determining the optimal model, we can use the Viterbi algorithm [*Viterbi*, 1967; *Forney*, 1973] to find the single best state sequence for the given observations which describes the classification of the observations into distinct groups and the transitions among different groups. For example, one can refer to *Bebbington* [2007] for the implementation steps of the Viterbi algorithm for HMMs.

Another direct and important use of the model is to provide probabilistic forecasts of tremor activity. Given the history of the tremor activity until time $t-1$, we can provide probabilistic forecasts of the occurrence and location of the tremor activity at time t using the best model for each region. The forecasting algorithm is provided in Appendix B.

4 Data analysis for the Kii region

We first use the 2D HMM described in the previous section to analyze the non-volcanic tremors in the Kii region from 2001 to 2012. The model with the minimum BIC value has 17 states. Different spatial segments obtained from this model are classified in Figures 3 and 4. The spatial and temporal migration between segments is demonstrated by the Viterbi path with latitude and longitude time series (The pattern of the full record is provided in the supplementary file). The estimated probabilities $\hat{p}_i$ of tremor occurrence in each state i and stationary probabilities $\boldsymbol{\pi}$ of the Markov chain are shown in Table 1. Figure 5(b) shows that the expected recurrence periods of the states increase with the probabilities of tremor occurrence in the states, suggesting that segments with more intense tremor activity have longer recurrence intervals.

Based on the outputs in Table 1 and Figure 5(a), the 17 states identified from the Kii region are categorized into three types: episodic states, weak concentration states, and background states. Episodic states 1, 2, 5–14 feature high tremor activity (with $p_i \geq 0.1$) lasting for more than 4 hours on average. Weak concentration states 3, 4, 15 demonstrate either low tremor activity (with $p_i < 0.1$) or very short average sojourn times of less than 4 hours. The background states 16 and 17 either span across a large spatial region or have very long average sojourn times (more than 2 days). In the case of state 16 very low levels of tremor activity are seen and in state 17 sporadic

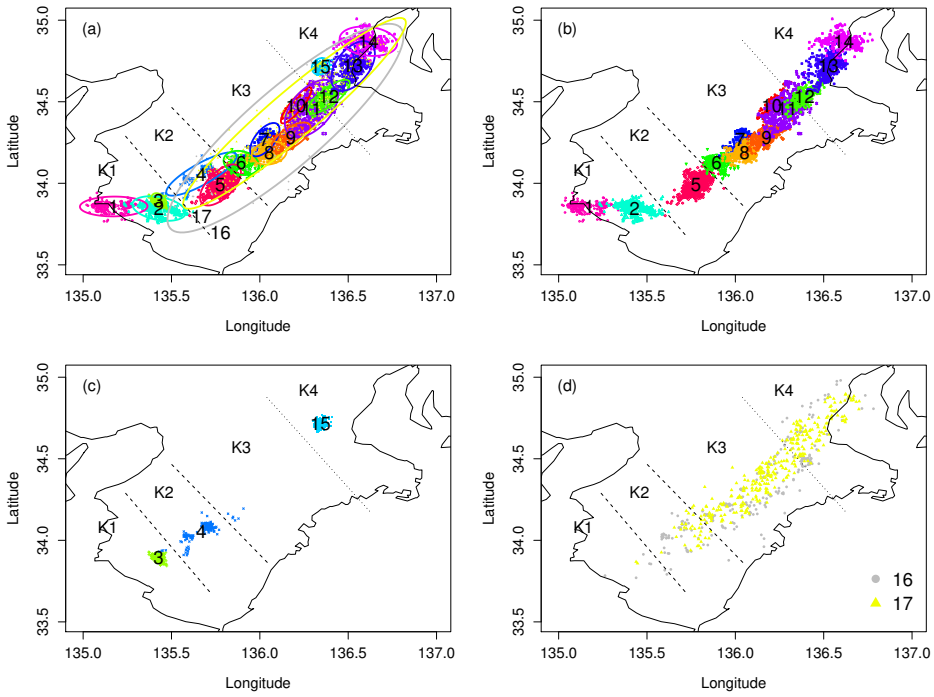

Figure 3. (a) Classification of distinct spatial segments of tremor events in the Kii region obtained from the 17-state 2D HMM; (b) episodic states; (c) weak concentration states; (d) background states. The points represent the hourly centroid locations of tremors for times when tremor occurred. State 16 is in gray and State 17 is in yellow.

Table 1. Parameter estimates from the 17-state HMM. S: state; $\hat{p}_i$: the estimated probability of observing a tremor event when the system is in state i; $\hat{\pi}_i$: the estimated stationary probabilities of the hidden Markov chain; $\hat{T}_S$: the average empirical sojourn times (in hours).

S	1	2	3	4	5	6	7	8	9	10
$\hat{p}_i$	0.161	0.378	0.368	0.069	0.645	0.261	0.218	0.635	0.712	0.366
$\hat{\pi}_i$	0.018	0.015	0.006	0.024	0.013	0.011	0.009	0.007	0.007	0.006
$\hat{T}_S$	14.0	10.6	2.8	7.6	8.0	17.6	8.7	9.6	5.2	8.7
S	11	12	13	14	15	16	17			
$\hat{p}_i$	0.684	0.573	0.595	0.238	0.378	0.002	0.902			
$\hat{\pi}_i$	0.007	0.007	0.008	0.013	0.005	0.841	0.004			
$\hat{T}_S$	10.9	7.8	8.6	14.1	3.1	178.0	2.7			

tremor occurs in east Kii (Figures 3, 4 and 5). In the following discussion, we will use state and segment interchangeably. When tremors in one state concentrate in space, we will mainly use segment. When tremors in a state span across a large area, we use state.

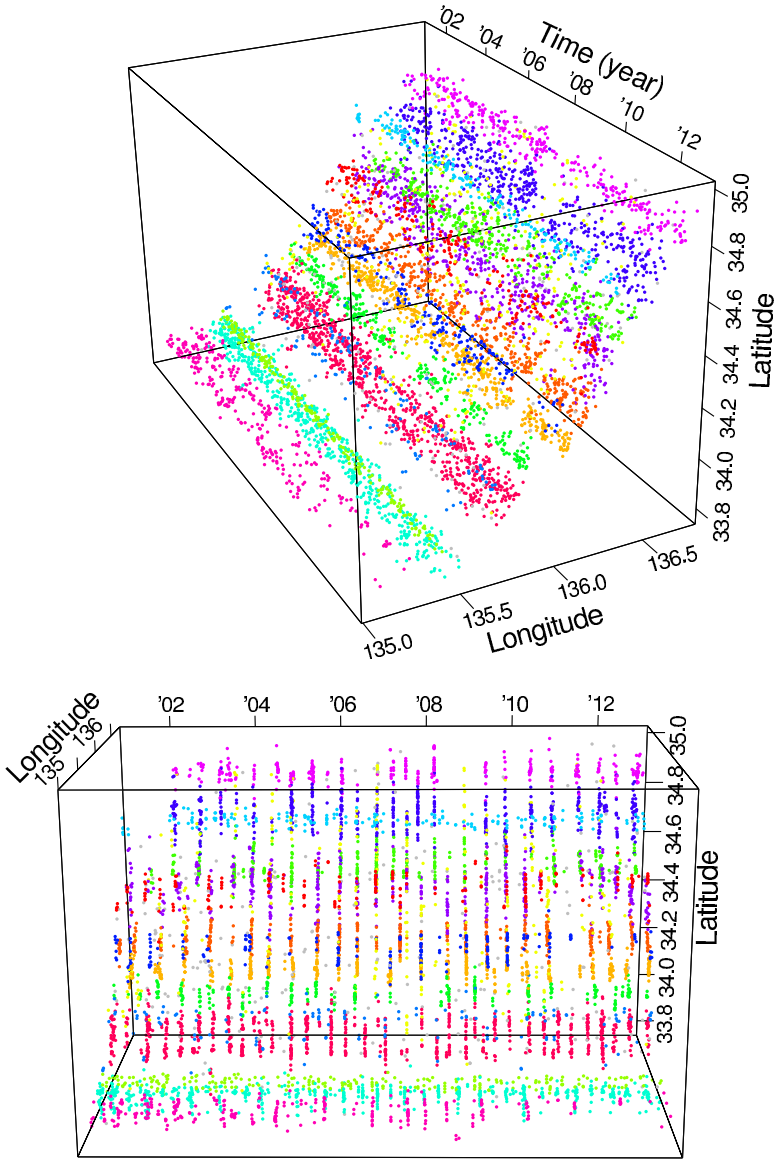

Figure 4. Spatiotemporal classification of distinct spatial segments of tremor events in the Kii region obtained from the 17-state 2D HMM.

4.1 Subsystems

Figure 6 plots the transition probabilities between states at consecutive times. Darker shading Figure 6(a) implies a higher transition probability. The grids appearing nearly blank suggest transition probabilities close to 0. At most times the system remains in its current state as represented by the dark diagonal elements. The transition probabilities suggest that the tremor activity in the Kii region can be divided into three main subsystems, among which one large subsystem sometimes splits into two. The first subsystem, namely K1, contains segments 1–3 and is spatially isolated from the major tremor sources to the northeast. The second subsystem consists of segments 4–5, where migration to the northwest occurs nearly twice as often as migration to the southeast. The third subsystem contains segments 6 to 15, featuring regular long-distance migration either from northeast to southwest or, less frequently,

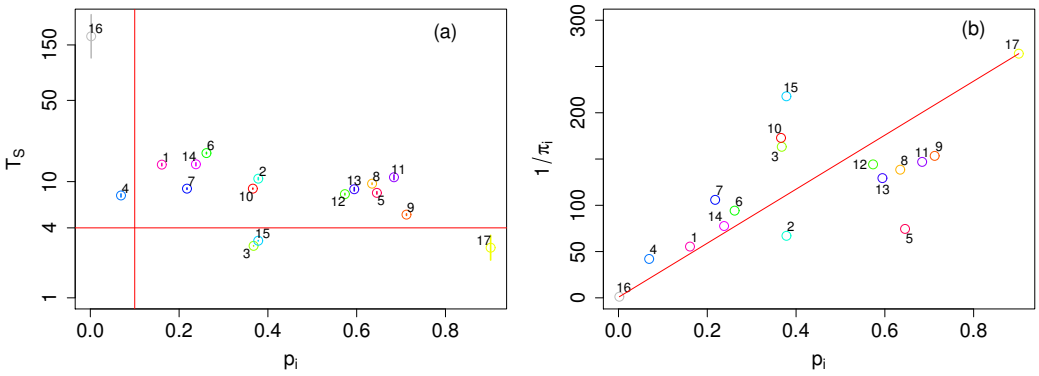

Figure 5. (a) Average empirical sojourn times in each state (in hours) against the estimated probability of observing a tremor event when the system is in each state for the Kii region. Vertical lines are proportional to the area of each confidence ellipse in Figure 3. (b) Estimated expected recurrence period for each state ($1/\pi_i$) against the estimated probability of observing a tremor event when the system is in each state.

in the opposite direction. This subsystem can be divided into two smaller subsystems K3 and K4, but the division is not as clear as among the other subsystems.

From the above division, we can see that the model clarifies the hierarchical structure present in the tremor activity. Within the Kii region different subsystems are present. Within each subsystem distinct spatial segments are identified. The probability that the tremor activity migrates across the subsystems is much lower than the probability that the tremor activity migrates between within-subsystem segments.

Subsystem K1 contains segments 1 to 3, with the highest rate of tremor occurrence in segment 2. Up-dip migration from segment 3 to 2 is more likely than down-dip migration. Tremor activity rarely migrates from segment 1 to 2. There are occasional westward migrations from segment 2 to 1, demonstrated in the Viterbi path (e.g. Jan 2002, Aug 2003, Oct 2005, Dec 2007, Feb 2009, Jan 2010 in the supplementary file). Segment 3 has a similar probability of tremor occurrence as segment 2, but it features isolated tremors and very short sojourn times (2.8 hours on average). It is worth noting that segment 3 has about one quarter the number of observations as segments 1 and 2.

Subsystem K2 contains the weak concentration segment 4, which has a low probability of tremor occurrence at 0.069, and highly active segment 5, where the probability of tremor occurrence is 0.645 with average sojourn time of 8.0 hours. The probability that the tremor activity transitions from segment 5 directly to segment 4 is 0.116, about twice as high as transitioning from segment 4 to 5. From Figure 3, we can see that segment 4 has three smaller sub-clusters, implying that the hierarchical structure can be detailed to another level.

A final large subsystem may be divided into two smaller subsystems although the boundary is not clear: subsystem K3 containing segments 6–12 and K4 including segments 11–15. Note that segments 11 and 12 could be associated with the tremor activity in both K3 and K4. There are some interesting migration patterns within subsystems K3 and K4. The tremor activity is unlikely to transition between segments 6 and 7, but more likely to transition between segments 6 and 8. Migration is most often in a southwest direction. Transition from state 7 is likely to be to state 9 and

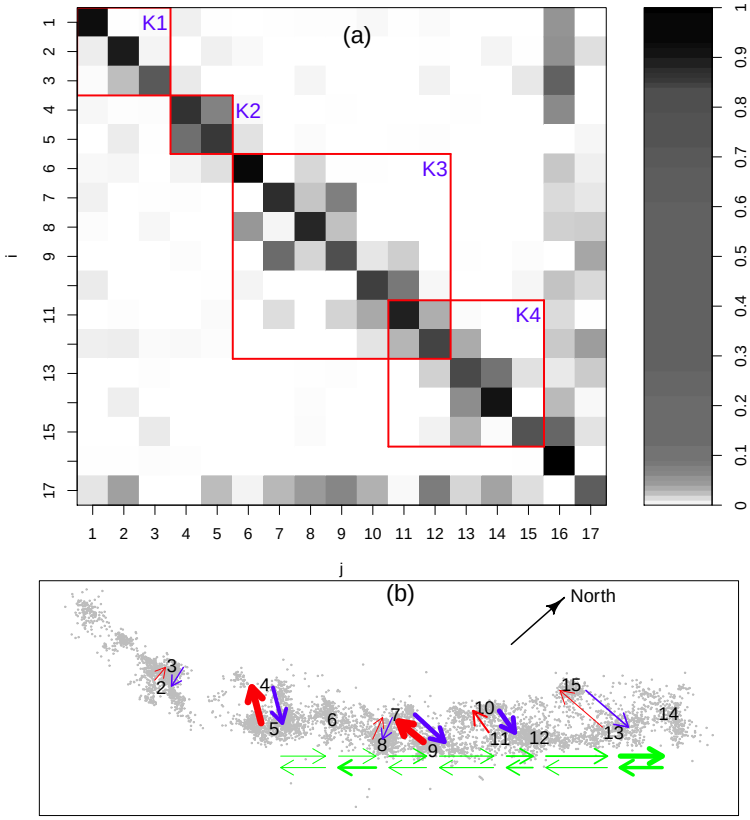

Figure 6. (a) The transition probabilities $\Pr\{S_t = j \mid S_{t-1} = i\} = \gamma_{ij}$ estimated from the 17-state 2D HMM for the Kii region. Darker shading implies a higher transition probability. The red rectangle corresponds to each subsystem. (b) Tremor migration patterns among segments. The whole map is rotated clockwise by 45°. The gray colored dots mark the tremor locations. The arrows indicate down-dip (red), up-dip (blue), and along-strike (green) migrations. The thickness of the arrows is proportional to the transition probabilities, i.e., thicker arrows mean higher proportions of migrations along the corresponding direction.

vice versa. Migration to or from segment 14 at the northeastern tip is mainly from or to the nearby segment 13. The weak concentration segment 15 has short sojourn times (3.1 hours on average). Up-dip migration from segment 7 to 8, 10 to 11 and from 15 to 13 is more likely than migration to the opposite direction.

Tremors in different subsystems are likely to be inter-related, and large tremor clusters in different subsystems may overlap. These subsystems are not independent of one another except the southwestern subsystem K1. There is strong evidence of spatiotemporal migration to the southwest from segment 14 at the far northeast tip of the system through 13, 12, 11, 10 and 9 to 7 in Jan 2004, Dec 2004, June 2006 and March 2008. We also see evidence of spatiotemporal migration of tremors in a northeast direction from segment 7 right through to 14 in the Viterbi plot in Jan 2006, May 2009 and Oct 2009. These examples provide evidence for a large subsystem containing both K3 and K4. However, we also see evidence of two separate processes in this larger subsystem when tremor clusters occur relating to K3 or K4 alone. Often, large tremor clusters migrate to both the northeast and the southwest from a central location.

The features of the four identified subsystems can be summarized as follows. Subsystem K1 can be considered independent of the tremor activity to the east of Kii. Within K1 we identify two major tremor sources (segments 1 and 2). Tremors often occur independently in the two tremor sources, although there is evidence of migration to the west sometimes. Subsystem K2 has both along-strike (see the analysis of East Kii region in the supplementary file) and along-dip (between segments 4 and 5 in Figure 3) migrations, which confirms the findings of *Obara et al.* [2012]. The probability of an along-strike migration to the southwest is similar to that of a migration to the northeast. Down-dip migrations are more likely than up-dip migrations in K2. Subsystem K3 has dominant migrations between segments 7 and 9 and between 6 and 8. We confirm the qualitative findings of *Obara* [2010] and *Obara et al.* [2012] that migrations along-strike to the southwest are more likely than to the northeast. Subsystem K4 features more along-strike migrations to both directions, also demonstrated in Figure 3 of *Obara et al.* [2012]. DIFaddDominant along-dip migrations in K3 and K4 are up-dip migrations.

We can also obtain more details about each individual segment. For example, the isolated small tremor clusters in segment 15 (Figure 3) locate at the deep part of the Kii region according to the isodepth contours in Figure 1 of *Obara et al.* [2010, 2012]. *Obara et al.* [2010] illustrated the bimodal distribution of the tremor activity in several empirically selected rectangular boxes along the dip direction in northern Kii. The HMM can clearly separate the segments in the down-dip and up-dip parts such as segments 7 and 9, 10 and 12 in Figure 3, and can provide details about the onset times of tremors in each of these segments. The weak tremors detected on the down-dip side of the Kii region in *Obara et al.* [2010] are clearly classified into segments 3, 4, and 15.

In summary, these quantitative confirmations demonstrate the reliability of the automated system in identifying migration patterns. Moreover, we can provide fast quantitative descriptions of the migrations and also gain further insight into the classification of tremor through the hierarchical structure and clustering of different types of tremor.

4.2 Tremor events outside of subsystems

The entire system is most often in state 16, suggested by the highest stationary probability among all the states in Table 1. It features the longest sojourn times, 178.0 hours on average, and covers a large geographical area. As the probability that tremor occurs in this state is very low at 0.002, it represents a background state or general quiescent state over the region.

In contrast, state 17 features the highest probability of tremor occurrence at 0.902 and the shortest sojourn times, 2.7 hours on average. It represents sporadic weak tremor occurrences across the region between episodic tremor states. State 17 covers a geographical area similar to the quiescent state 16. Tremors in this state are unlikely to be located in the west tip of the Kii region covered by segments 1–3.

4.3 Temporal variation of occurrence rate

We used a constant p_i to model the probability that tremors occur in each state, but can still investigate temporal variation in this probability without introducing more parameters and increasing the complexity of the model. After using the Viterbi path to categorize the data into different spatiotemporal clusters, we can calculate the proportion of tremors observed in each state in evenly divided time intervals of one year each. These proportions characterise the concentration of tremor activity over time in each segment. The results in Figure 7 show some cyclic patterns in segments 8, 9, 11, and 12, which may be sinusoidal but with 12 years of data it is difficult to validate. We

also see that there are times when the rate of tremor activity is significantly different, for example comparing the third and fifth time intervals in segment 3.

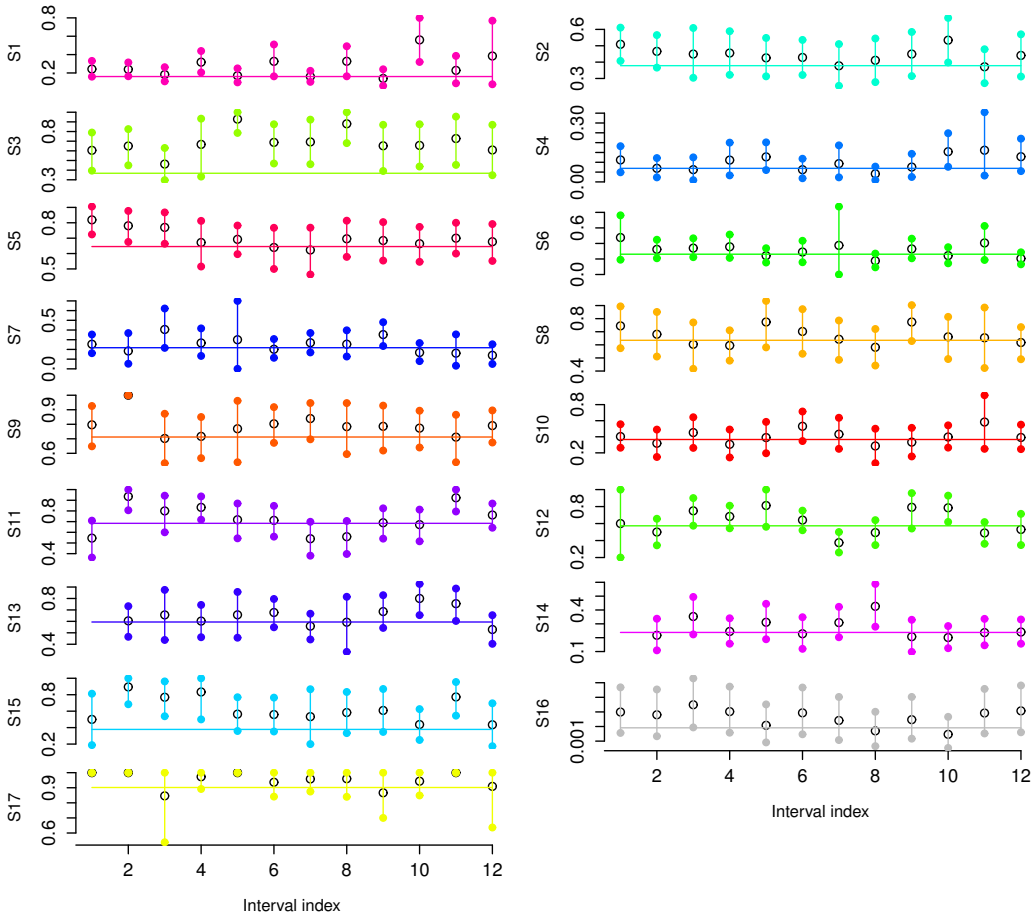

Figure 7. The proportion of tremors in each state over 12 intervals for the Kii region. Each interval is about one year. Each circle indicates the proportion of tremors in each state in that interval obtained from the Viterbi path. The vertical bar shows the 99% confidence interval of this proportion. The horizontal line represents the estimated $\hat{p}_i$ from the HMM.

4.4 Relation to short-term slow slip events

To examine the temporal variation of the three types of tremor in relation to the short-term slow slip events recorded in *Sekine et al.* [2010], we plot the proportion of each type of tremor events out of the total number of tremor events in each day in Figure 8. For days when no tremor occurred, the proportion in those days is not available and is thus shown as blank in the plot.

Among the 12 slow slip events listed in *Sekine et al.* [2010], 6 had high proportions of tremor from weak concentration states in the two weeks prior to or at the onset of slow slip. During slow slip, the system mainly stays in highly active episodic states with occasional transitions to background states, but rarely enters weak concentration states. Four out of the 12 slow slip events were followed by tremors from weak concentration states in the 7 days after slow slip or at the end of slow slip. We also see in many cases that high proportions of tremor from episodic states immediately precede

or follow slow slip events. This indicates that slow slip may have occurred earlier or finished later than determined in *Sekine et al.* [2010]. Currently the timing of slow slip events cannot be determined to the hour using geodetic data. However, new research in this field combining geodetic and tremor data may provide higher-resolution timing of slow slip events in the future. When more data with higher temporal resolution are available, the classification of segments in space and time from the HMM provides a straightforward route for us to study systematically the correlation between slow slip events and tremors in different segments, subsystems, or types.

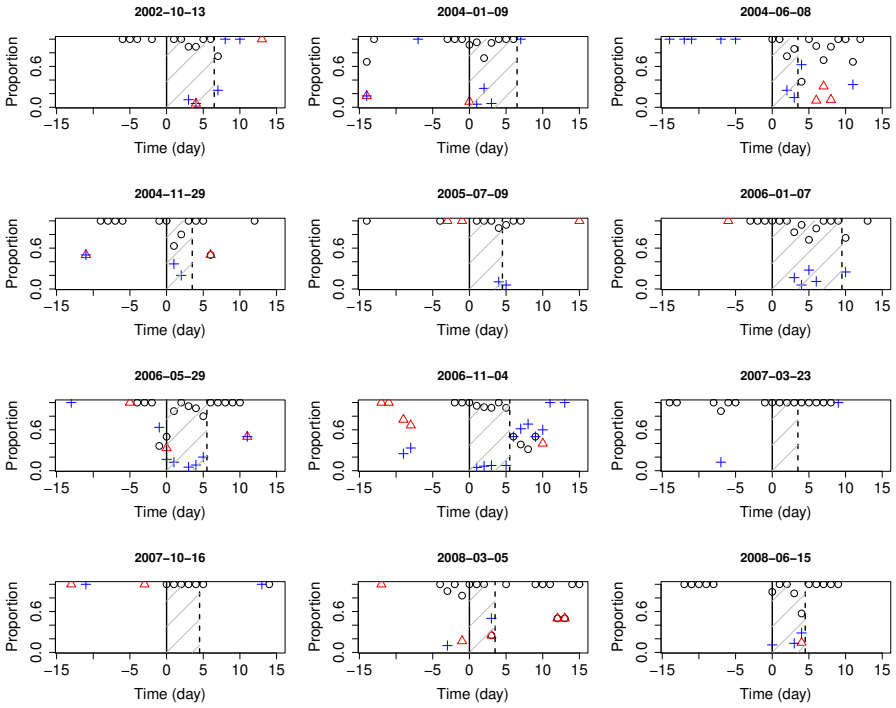

Figure 8. Proportion of each type of tremor events out of the total number of tremor events in each day before, during and after each short-term slow slip event listed in Sekine et al. (2010) in the Kii region. Solid vertical lines at time 0 indicate the onset times of slow slip events, the dates of which are also shown above the plots. Dashed vertical lines indicate the end of slow slip events. Black circles: tremors from episodic states; red triangles: tremors from weak concentration states; blue crosses: tremors from background states.

4.5 Forecasting

To visualize the performance of probabilistic forecasts from this model, we forecast the probability density of tremor occurrence and the locations of tremors. We carry out forecasts for a randomly chosen period of 48 hours (March 13 14:00 to March 15 13:00 2002) when tremor activity was present using the algorithm described in the end of Section 3 and Appendix B. Figure 9 shows the actual location of tremor occurrences in the chosen 48 hour period (red dots) along with the forecast probability density of locations. Deeper colour indicates higher probability of tremor occurrence at that location. We can see that the forecast density agrees well with the observed locations.

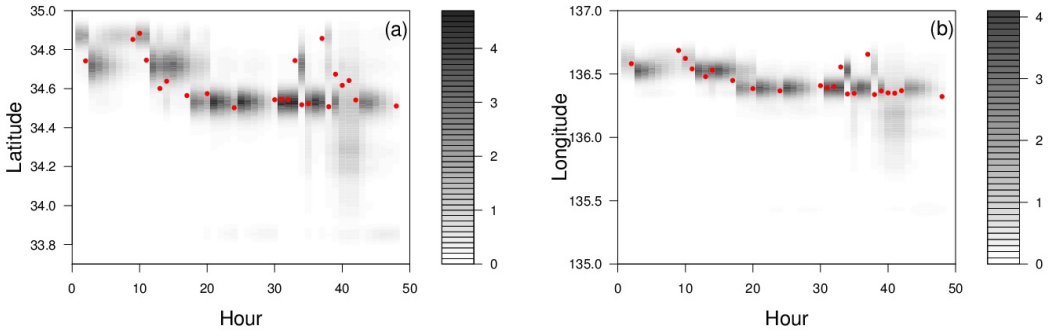

Figure 9. Forecast probability density of tremor occurrence times and locations and the observed tremor occurrence times and locations (red dots) in the Kii region.

We can also compare our model with a null model in their performance in forecasting occurrences and locations of tremors using information gain as described in Section 4.3 of *Wang et al.* [2016]. The null model that we consider assumes that tremors are independent and identically distributed, the probability of tremor occurrence at any time is p_0, and the locations of tremors are independent and identically distributed with a density function $g(x)$. The quantities p_0 and $g(x)$ can be estimated by using

$$\begin{aligned} \hat{p}_0 &= N/T, \\ \hat{g}(x) &= \frac{\text{number of tremors in } \Delta\mathbf{x}}{|\Delta\mathbf{x}|N} \end{aligned}$$

where N is the total number of tremor events, T is the total number of time points, $\Delta\mathbf{x}$ is a small grid cell, and $|\Delta\mathbf{x}|$ is the area of the grid cell. For further details readers are referred to Section 4.3 of *Wang et al.* [2016].

The information gains per time point and per tremor event are 0.167 and 2.53 respectively, when we divide the Kii region into 50×50 grid cells of equal sizes. To test the sensitivity of the sizes of grid cells, we tried different divisions ranging from 20×20 to 100×100 grid cells. The range of the corresponding information gain per time point is between 0.155 and 0.189. The range of the information gain per tremor event is between 2.32 and 2.89. This means that on average the likelihood ratio of our model against the null model is about $\exp(2.53) = 12.55$ per event.

In summary, the HMM model provides good forecasts of future tremor activity in the Kii region. As discussed in Section 4.4, when we can further establish relationships between tremor and slow slip, this model can be used to forecast slow slip events based on their relationship with tremor. In general, the differences between forecasts and real occurrences (residuals) provide hints of directions to improve the model or to study the physical reasons that cause such discrepancies.

5 Data analysis for the Shikoku Region

In our initial study of the entire data set in the Shikoku region using the method described in Section 3, we find that the cluster to the northeast tip of this region (yellow dots in Figure 1) forms a segment with spatially concentrated tremors that are independent from the tremor activity in the other segments. We therefore re-analyze the data excluding tremors from this segment given that before and after the tremor occurrences in this segment, there is most likely a period of quiescence in western part of Shikoku.

The 2D HMM for the tremor data in the Shikoku region with the minimum BIC value has 25 states. Different spatial segments obtained from this model are classified in Figures 10 and 11. The spatial and temporal migration pattern is demonstrated by the Viterbi path with latitude and longitude time series (see the supplementary file for the pattern of the full record). The estimated probabilities of tremor occurrence, $\hat{p}_i$, in each state i and stationary probabilities, $\boldsymbol{\pi}$, of the Markov chain are shown in Table 2.

Similar to the Kii region, segments with more intense tremor activity have longer recurrence intervals (Figure 12(b)). On average tremor clusters last longer in the Kii region than in the Shikoku region (Figures 5 and 12). Many segments in Shikoku are long and thin, such as segments 3, 5, 16, 23, 24, with orientation either along the direction of the current or past plate motion more than 3 to 5 million years ago [*Ide*, 2010]. Segments 5 and 23 correspond to the clusters of tremors with deep average depth in Figure 1 in *Ide* [2010].

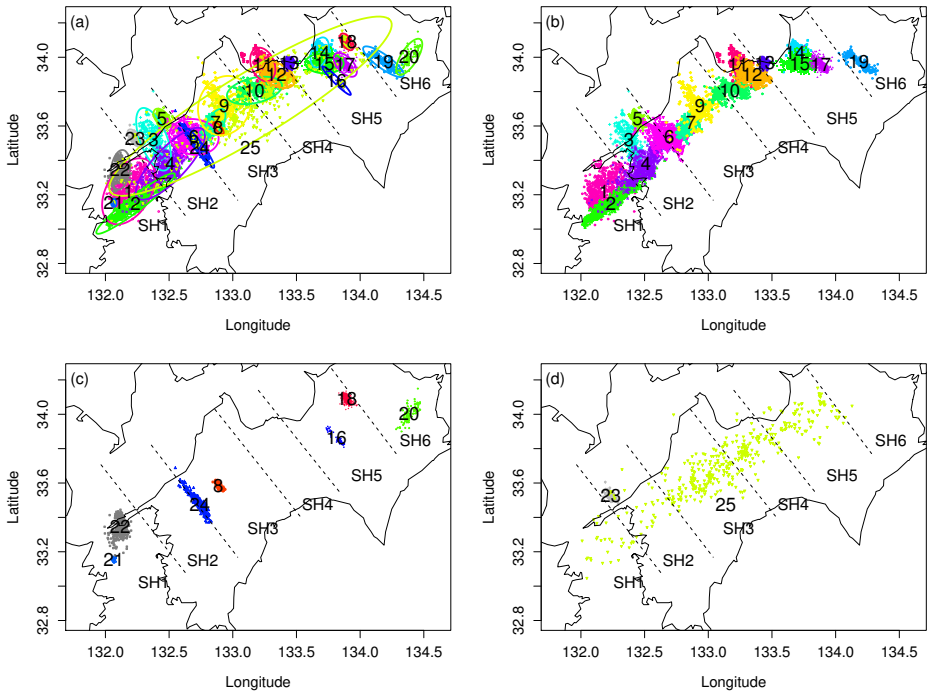

Figure 10. (a) Classification of distinct spatial segments of tremor events in the Shikoku region obtained from the 25-state 2D HMM; (b) episodic states; (c) weak concentration states; (d) background states. The points represent the hourly centroid locations of tremors for times when tremor occurred. The light green squares scattered in SH3, SH4, and SH5 belong to state 25.

The 25 states identified from the Shikoku region are also categorized into three types (Table 2 and Figure 12(a)). States 1–7, 9–15, 17, anvd 19 featuring high tremor activity (with $p_i \geq 0.1$) and lasting for more than 3 hours on average are episodic. Weak concentration states 8, 16, 18, 20, 21, 22, and 24 show either low tremor activity (with $p_i < 0.1$) or very short average sojourn times of less than 3 hours. Background states 23 and 25 either cover a large geographical region or have very long average sojourn times (more than 2 days). Note that state 17 has average empirical sojourn time of 2.7 hours that is close to the border line of our cutoff for the three types of

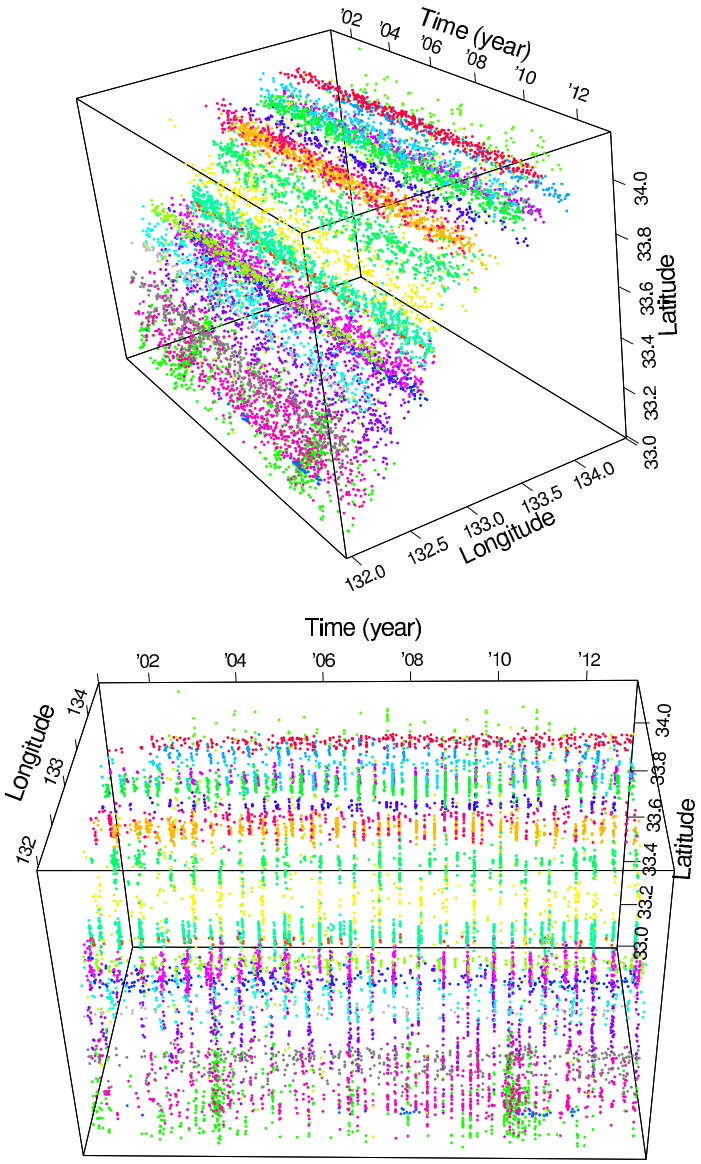

Figure 11. Spatiotemporal classification of distinct spatial segments of tremor events obtained from the 25-state 2D HMM.

tremor. However, since it has a very high probability of tremor occurrence (over 0.8), we regard it as episodic.

5.1 Subsystems

Based on the transition probabilities shown in Figure 13, we identified six subsystems in the Shikoku region. They are classified as segments 1–2 (SH1), segments 3–5 (SH2), segments 6–9 (SH3), segments 9–12 (SH4), segments 13–18 (SH5), and segments 19-20 (SH6). Subsystems SH2 and SH3 sometimes occur as one large subsystem as suggested by the darkish grey cells (i.e., non-negligible probability of transition) between states 6 and 4, 4 and 8.

Table 2. Parameter estimates from the 25-state HMM for the Shikoku region. S: state; $\hat{p}_i$: the estimated probability of observing a tremor event when the system is in state i; $\hat{\pi}_i$: the estimated stationary probabilities of the hidden Markov chain; $\hat{T}_S$: the average empirical sojourn times (in hours).

S	1	2	3	4	5	6	7	8	9	10
$\hat{p}_i$	0.748	0.211	0.447	0.441	0.473	0.785	0.679	0.050	0.705	0.604
$\hat{\pi}_i$	0.011	0.032	0.008	0.016	0.006	0.011	0.014	0.033	0.005	0.011
$\hat{T}_S$	5.1	10.6	5.1	11.5	4.0	4.0	5.3	8.7	4.1	4.1
S	11	12	13	14	15	16	17	18	19	20
$\hat{p}_i$	0.409	0.789	0.560	0.388	0.843	0.031	0.829	0.074	0.471	0.046
$\hat{\pi}_i$	0.008	0.010	0.003	0.008	0.009	0.023	0.004	0.048	0.005	0.021
$\hat{T}_S$	4.1	5.0	3.2	5.4	4.5	10.1	2.7	13.5	3.5	18.8
S	21	22	23	24	25					
$\hat{p}_i$	0.008	0.604	0.001	1.000	1.000					
$\hat{\pi}_i$	0.042	0.006	0.660	0.003	0.004					
$\hat{T}_S$	11.5	2.1	69.2	1.1	1.4					

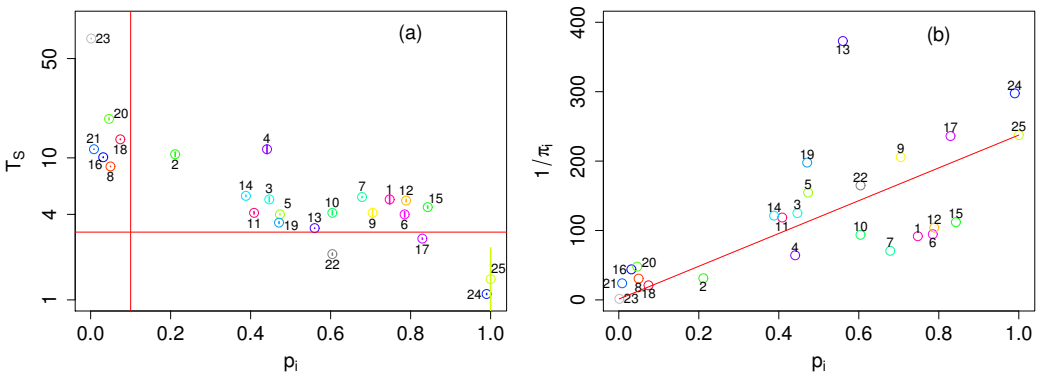

Figure 12. (a) Average empirical sojourn times in each state (in hours) against the estimated probability of observing a tremor event when the system is in each state for the Shikoku region. Vertical lines are proportional to the area of each confidence ellipse in Figure 10. (b) Estimated expected recurrence period for each state ($1/\pi_i$) against the estimated probability of observing a tremor event when the system is in each state.

Subsystem SH1 (segments 1 and 2) to the southwest of the Shikoku region is most active in segment 1 where the probability of tremor occurrence is 0.748 (see Table 2). The probability that the tremor activity transitions from segment 1 to the significantly less active segment 2 is nearly three times the probability of a migration from 2 to 1. A number of tremor clusters in segments 1 and 2 have a recurrence period of approximately two months.

The subsystems SH2 (segments 3 to 5) and SH3 (segments 6 to 9) often occur as one large subsystem. The two smaller subsystems have different probabilities of tremor occurrence, with higher probability in SH3. All three segments in SH2 have similar probabilities of tremor occurrence around 0.45 (see Table 2), although segment

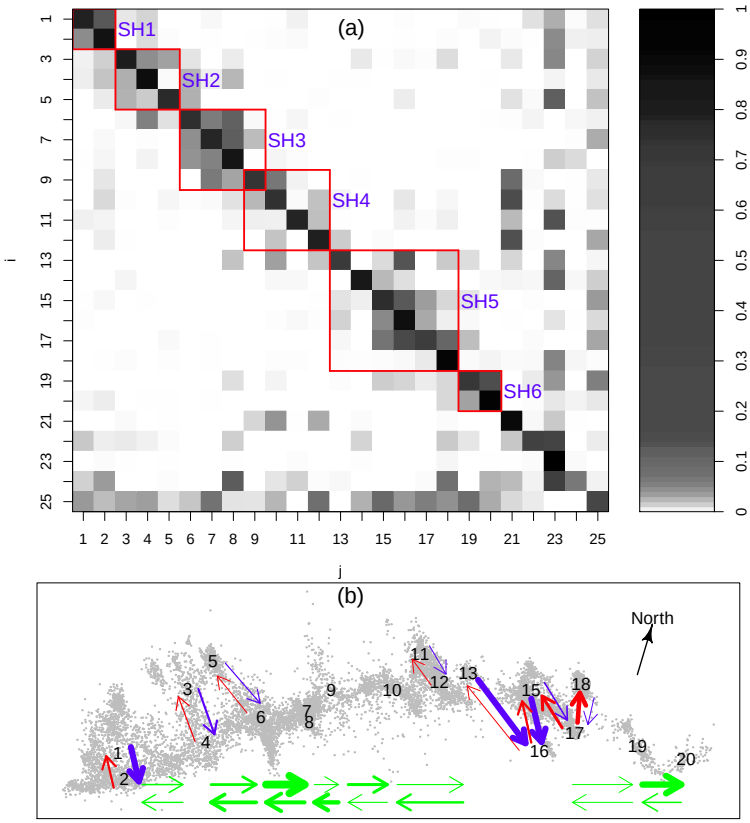

Figure 13. (a) The transition probabilities $\Pr\{S_t = j \mid S_{t-1} = i\} = \gamma_{ij}$ estimated from the 25-state 2D HMM for the Shikoku region. Darker shading implies a higher transition probability. The red rectangle corresponds to each subsystem. (b) Tremor migration patterns among segments. The whole map is rotated clockwise by 20°. The gray colored dots mark the tremor locations. The arrows indicate down-dip (red), up-dip (blue), and along-strike (green) migrations. The thickness of the arrows is proportional to the transition probabilities, i.e., thicker arrows mean higher proportions of migrations along the corresponding direction.

5 is much more compact in space. The segments in subsystem SH3 also have similar probabilities of tremor occurrence (around 0.7) except the weak concentration segment 8 (around 0.05).

Sometimes the two smaller subsystems SH2 and SH3 occur separately. In SH2, up-dip migration patterns (i.e., from segments 3 and 5 to 4) occur nearly twice as frequently as down-dip migration patterns. The time spent in segment 4 is more than twice the time spent in segment 3 or 5.

In subsystem SH3, the recurrence period for segment 9 is around 6 months, and for segments 6 and 7 is shorter, around every 3 months. There seem to be few direct migrations of tremor activity between the two spatially larger segments 6 and 9. The transition probabilities in Figure 13 suggest that when the tremor activity in this subsystem migrates to the northeast, it often stops in the weak concentration segment 8 without entering into segment 9. However, when the migration is from northeast to southwest, it often goes from segment 9, through segments 8 and 7, and to segment 6. Without considering the weak concentration segment 8, the probability of transitioning from segment 9 to 7 is nearly three times that from 7 to 9. Migrations to the northeast

appear to occur more often around August and September, while westerly migrations occur more often from December to February. There are obvious exceptions to this such as in February 2002 as well as May and October 2004.

Subsystem SH4 contains four segments including 9, which is shared with SH3, and 10-12, with short sojourn times of around 4 hours on average. This subsystem is linked to subsystem SH3 through the migrations between segments 9 and 10. The probability of migration from segment 9 to 10 is nearly three times that from 10 to 9, suggesting that migration to the northeast is more likely than to the southwest in this part of the subsystem. Referring to the transition probability plot (Figure 13), we see that migration from segment 12 to 11 is rare. Migrations from segment 11 to 12 are more common.

Subsystem SH5 (segments 13 to 18) is in Central Shikoku. The recurrence period for the large clusters in this subsystem appears to be somewhere in the region of 3 to 4 months. Note that the transition probability matrix in Figure 13 suggests a stronger association between segment 13 and the other segments in SH5, although there are some transitions between segment 13 and the segments in SH4. The number of observed tremors in segment 13 is only 160, approximately 1.5% of the total 11012 hours with tremor occurrence in the Shikoku region. On some occasions there is clear spatiotemporal migration to the southeast from segment 14 to 15 then to 17 and weak concentration segment 16, such as in Aug 2001 and Dec 2003. The transition probabilities in Figure 13 suggest dominant up-dip migration from segments 13 and 15 to 16, and northward migration from segment 17 to 18.

In subsystem SH6 (segments 19 and 20), segment 19 has very short sojourn times (3.5 hours on average) and high probability of tremor occurrence at 0.471; whereas segment 20 has long sojourn times (18.8 hours on average) and a probability of tremor occurrence as low as 0.046. Tremor activity is more likely to transition from segment 19 to weak concentration segment 20 than from 20 to 19. The connection between SH6 and SH5 is through migrations between segment 19 and any of the nearby segments 13, 15, and 17.

Tremors in the six subsystems are not entirely independent, but linked with along-strike migration of tremor activity in neighboring subsystems. The most obvious link is between subsystems SH2 and SH3, where slow slip events have likely facilitated the smooth migration of tremors in the two subsystems. Within SH2 and SH3 migration to the northeast is more likely than to the southwest as also shown in *Obara* [2010]. Migration to the northeast is more likely between SH3 and SH4. For example, the probability of a transition from state 9 to state 10 is 0.065 compared to 0.024 from state 10 to 9. Migration between SH4 and SH5 is mainly through segment 13, with migration to the southwest more likely. The division of subsystems SH4 and SH5 confirms the discussion in *Obara et al.* [2011] where the authors found that cluster B (segment 13 in SH5) occurs at the same time as cluster C (segments 14–18 in SH5). Migration between SH5 and SH6 is more likely to eastward which agrees with *Obara* [2010].

In addition to the above along-strike migrations, the transition probabilities between segments in each subsystem also reveal along-dip migration. In subsystems SH1 and SH2, up-dip migrations are nearly three times and twice more likely than down-dip migrations, respectively. The along-dip migration in subsystem SH4 is mainly up-dip. The findings are consistent with those of *Obara et al.* [2011] and specify estimated probabilities for transitions between neighboring states at the edges of the subsystems. Furthermore, most major migrations in SH5 are up-dip migrations along the segments 14–16 and 13 to 16. There are also significant down-dip migrations along segments 17 and 18.

5.2 Tremor events outside of subsystems

Segments 22 and 24 are weak concentration states containing regular isolated tremors. These segments are geographically small with very short sojourn times. State 25 is a background state corresponding to occasional sporadic occurrences of weak tremors. The sojourn time for state 25 is often 1 hour. Tremors in this state are located throughout the region although they are mostly concentrated in the central portion. State 23 is the main background state with very low probability of tremor occurrence at 0.001 and long sojourn times of 69.2 hours on average. At most times the system in the Shikoku region is quiescent in the background state 23 interspersed with some isolated tremors and larger tremor clusters which migrate over time within the system.

A number of weak tremor segments with either very low probability of tremor occurrence or short sojourn times are mainly situated to the down-dip side or to the east of Shikoku (segments 18, 20–23 in Figure 10) except segments 8, 16, and 24 that lie in long and thin bands perpendicular to the strike. The isolated tremors in these segments recur more frequently than large tremor clusters and the average recurrence periods are in the range of 1.5 days to 1.5 months. These weak segments identified by the HMM confirm the location of weak tremor activity provided in the heat map from Figure 1 in *Obara et al.* [2011]. *Obara et al.* [2011] divided the entire Shikoku region into $0.03^\circ \times 0.03^\circ$ grid cells and calculated the ratio of major tremor activity lasting more than 24 hours in each grid cell. Our HMM method can provide clear spatial boundaries and onset and ending times of these weak segments.

5.3 Temporal variation of occurrence rate

The proportion of tremors observed in each state in evenly divided 12 time intervals (1 year in each interval) is shown in Figure 14. We see that the proportion of tremor occurrence in some segments changes over time, sometimes significantly. For example, there is evidence of cyclical behaviour in segments 1, 2, 5, 6, 11, 12, 13, 15, and 19, which may be sinusoidal but again with 12 years of data it is difficult to validate. Of special interest is the pattern in segment 2. We see an increasing proportion of tremor occurrences prior to 2003 and 2010. This is likely to be related to the two long-term slow slip events in 2003 [*Ozawa et al.*, 2004; *Hirose and Obara*, 2005] and 2010 [*Hirose et al.*, 2010] that occurred close to segment 2. Such increase is also visible in segment 1 before 2003 and in segment 21 before 2010. According to the position of the slow slip event in 2003 in Figure 7 in *Obara* [2011], this slow slip event also affected segment 1.

5.4 Relation to short-term slow slip events

Figure 15 shows the temporal variation of the proportion of each type of tremor events out of the total number of tremor events in each day in relation to the short-term slow slip events recorded in *Sekine et al.* [2010] in the Shikoku region. Nineteen of the 21 slow slip events had high proportions of tremor from weak concentration states during the two weeks prior to or at the onset of slow slip. Similar to the Kii region, during the time period of slow slip, there is rarely a high proportion of tremor occurrence from weak concentration states.

At this stage, it is difficult to draw further systematic conclusions between slow slip events and tremors. This is because the exact start times for the slow slip events in terms of hours are still difficult to obtain due to the precision of and noise in the geodetic data used in the calculation. However, if slow slip data with higher temporal resolution are available, then we can find the proportion of slow slip events that are preceded by weak concentration tremor states. Using this, slow slip events could be

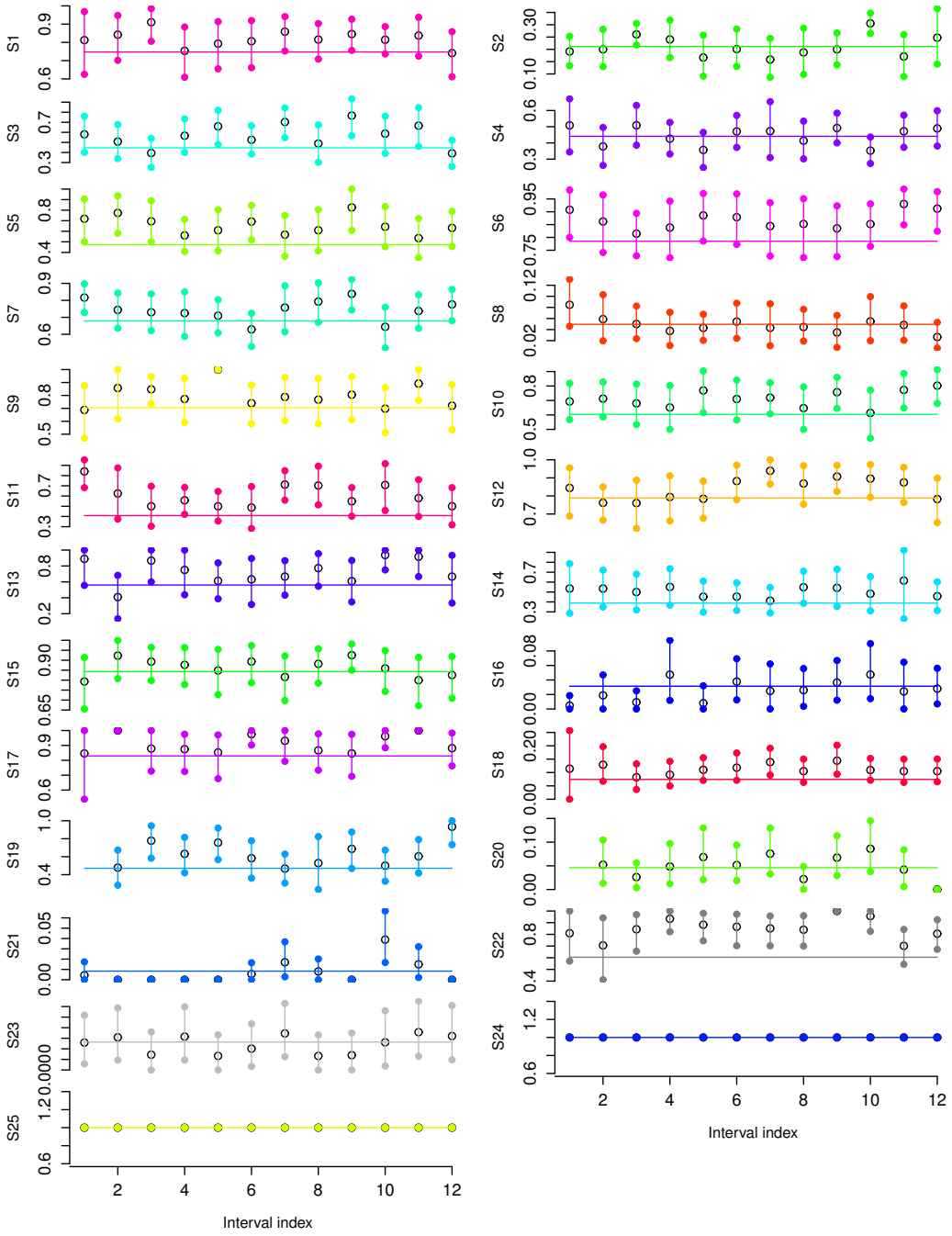

Figure 14. The proportion of tremors in each state over 12 intervals for the Shikoku region. Each interval is about one year. Each circle indicates the proportion of tremors in each state in that interval obtained from the Viterbi path. The vertical bar shows the 99% confidence interval of this proportion. The horizontal line represents the estimated p_i from the HMM.

forecast probabilistically. With further advances in technology and techniques, more effort should be put in this direction.

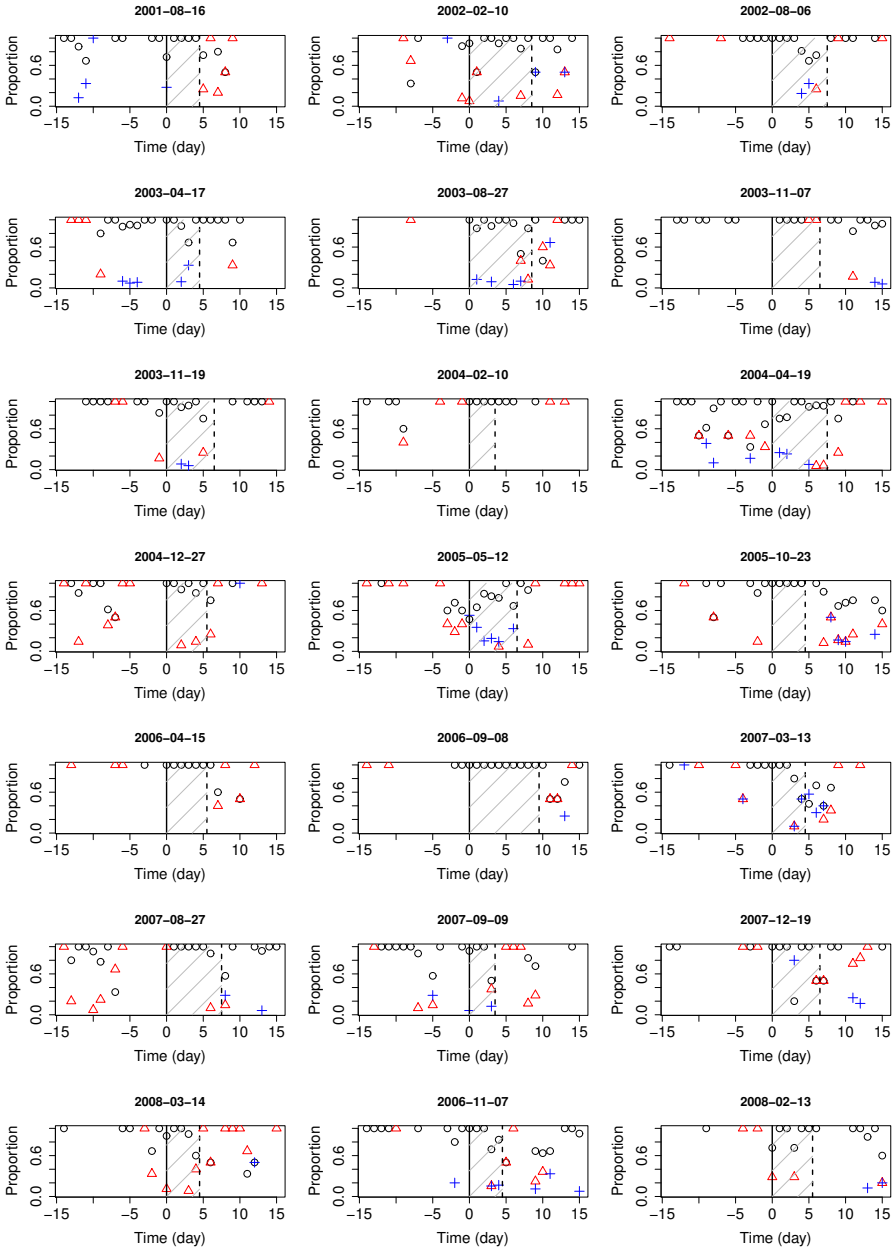

Figure 15. Proportion of each type of tremor events out of the total number of tremor events in each day before, during and after each short-term slow slip event listed in Sekine et al. (2010) in the Shikoku region. Solid vertical lines at time 0 indicate the onset times of slow slip events, the dates of which are also shown above the plots. Dashed vertical lines indicate the end of slow slip events. Black circles: tremors from episodic states; red triangles: tremors from weak concentration states; blue crosses: tremors from background states.

5.5 Forecasting

We also carry out probabilistic forecasts from this model for a period of 48 hours (January 3 18:00 to January 5 17:00 2001) when tremor activity is present. Figure 16 shows the actual locations of tremor occurrences (red dots) in the chosen 48 hour

period along with the forecast probability density of locations. We can see that the forecast density agrees well with the observed locations. The model is able to provide efficient probabilistic forecasts of future tremor occurrences and their locations.

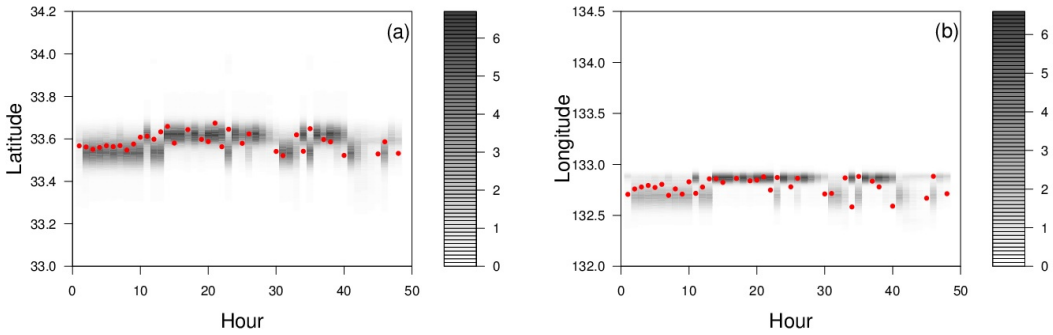

Figure 16. Forecast probability density of tremor occurrence times and locations and the observed tremor occurrence times and locations (red dots) in the Shikoku region.

Similar to the analysis for the Kii region, the information gains per time point and per tremor event are 0.242 and 2.11 respectively, when we divide the Shikoku region into 50×50 grid cells of equal size. To test the sensitivity of the sizes of grid cells, we tried different divisions ranging from 20×20 to 100×100 grid cells. The range of the corresponding information gain per time point is between 0.221 and 0.281. The range of the information gain per tremor event is between 1.91 and 2.48. This means that on average the likelihood ratio of our model against the null model is about $\exp(2.11) = 8.25$ per event.

6 Discussion

6.1 Comparison with the existing literature: what we confirmed

We quantitatively confirmed many findings from previous studies. We clearly separated the segments in the down-dip and up-dip parts of Kii region and found that tremor segments located to the down-dip on average have lower occurrence rates than those located to up-dip, which confirms that up-dip tremor activity is more episodic than down-dip activity as shown in *Obara et al.* [2010]. The along-strike and along-dip migrations demonstrated in *Obara et al.* [2012] are confirmed by the probabilities of transitions between different segments in Figure 6. Up-dip migrations from segment 3 to 2, 7 to 8, 10 to 11 and 15 to 13 in subsystems K1, K3 and K4 are more likely than down-dip migrations. This is consistent with the discussions in *Obara et al.* [2012]. In subsystem K2, however, down-dip migrations are more likely than up-dip migrations, and along-strike migration to the southwest is as likely as to the northeast. The probability of along-strike migrations to the southwest in subsystem K3 is higher than that to the northeast, which confirms the findings of *Obara* [2010] and *Obara et al.* [2012].

Figure 13 indicates dominant up-dip migrations in SH1, SH2, SH4, and SH5. For example, up-dip migrations are nearly three times and twice more likely than down-dip migrations in subsystems SH1 and SH2 respectively. *Obara et al.* [2011] found that Cluster A (corresponding to SH4) mostly consists of up-dip migrations, which is confirmed by the nearly negligible transition from segment 12 to 11 compared to from 11 to 12 in SH4 (Figure 13). These dominant up-dip migration patterns of tremor

activity in both Kii and Shikoku regions are also consistent with the findings in *Wech and Creager* [2011], which are related to stress transfer to the up-dip seismogenic zone. Figure 13 also suggests that along-strike migration in Western and Eastern Shikoku is more likely to the northeast, which agrees with *Obara* [2010]. More specifically, we found that northeastward migration from SH2 to SH3, within SH3, from SH3 to SH4, and from SH5 to SH6 is more likely than to the opposite direction. Southwestward migration from SH5 to SH4 is more likely than from SH4 to SH5. We also confirmed the division of subsystems SH4 and SH5 as discussed in *Obara et al.* [2011].

6.2 Comparison with the existing literature: new findings

Many new features of tremor activity are found in this study. First of all, tremor activity can be grouped into spatial subsystems, four subsystems in the Kii region and six in the Shikoku region. Each subsystem consists of several distinct spatial segments of tremor activity. Tremor activity migrates more frequently between spatial segments within each subsystem than across different subsystems. Some of the subsystems overlap in space and are linked by across-subsystem migration of tremor activity as shown in Figures 3, 6, 10, and 13. This suggests that some spatial subsystems occur more independently from other tremor activity in the same geographical region. The grouping of subsystems can help us objectively divide the region into subregions, and hence enable more detailed study of the properties of tremor activity in each subregion individually in the future. When dividing overlapping subsystems, care should be taken to make sure that the spatial segments that link two subsystems are considered in both subsystems. In other words, if we split these spatial segments somewhere in the middle to divide the two subsystems, some migration information will be lost.

Spatiotemporal segments of tremor activity in the Kii and Shikoku regions are classified into three types: episodic segments featuring high tremor activity, weak concentration segments with either low tremor activity or very short average sojourn times, and background activity either spanning across a large spatial region or having very long average sojourn times. The concentration of tremor activity over time in central Kii region (episodic segments 8, 9, 11, and 12 in subsystem K3 shown in Figure 3) and in many segments in the Shikoku region (episodic segments 1, 2, 5, 6, 11, 12, 13, 15, and 19 shown in Figure 10) show some cyclic patterns. The patterns may be sinusoidal but it is difficult to validate with 12 years of data.

In both regions, tremor from weak concentration segments often occurred during the two weeks prior to or at the onset of short-term slow slip events or followed short-term slow slip events listed in *Sekine et al.* [2010], but rarely occurred during the time period of slow slip. During slow slip, active tremor activity occurred in episodic segments with occasional transitions to background activity, but we rarely see tremor activity in weak concentration segments. There is a possibility that slow slip have occurred earlier or finished later than determined in *Sekine et al.* [2010]. This suggests a need to design improved models to provide higher-resolution timing of slow slip events in the future by combining geodetic and tremor data.

6.3 On data quality

In this study, we used the hourly centroid catalog determined using the clustering method as described in *Obara et al.* [2010]. According to *Annoura et al.* [2016], while some energy released from high-amplitude tremors was not entirely captured in the catalog from *Obara et al.* [2010], whether tremor occurred in each hour was well detected. Some tremor events with high amplitudes may have been missing from the catalog, especially in the western edge of the Shikoku region, and the corresponding hours are treated as zero (absence of event) in our model. Our study only considered the location of tremor in each hour. Therefore, the energy calculation has negligible

influence on the results from our model, whereas the missing data may cause underestimation of the proportion of tremor occurrence in each segment.

This method can also be applied to catalogs in a smaller spatial region with higher temporal resolution such as tremor locations in each minute. However, due to larger uncertainties in the locations determined in each minute than that in the centroid locations of tremor events determined in each hour, it is difficult to judge to what degree the use of data in each minute helps identify more detailed features of tremor segmentation.

6.4 Why is an automated model necessary?

The main advantage of using the HMM is that the model automatically classifies these segments and provides an objective boundary for each segment. The transition probability matrix expands our understanding about temporal migrations of tremor activity between segments and aids the definition of subsystems. A clear indication of the number of segments and their relationship to each other has not been possible with previous methods. In addition, we are able to further analyze each classified segment to better understand the properties of each segment of tremor sources. For example, the cyclical patterns identified in the observed proportion of tremors in some segments for both the Kii and Shikoku regions, as seen in Figures 7 and 14, may be related to the short-term and long-term slow slip events in the regions. This suggests that the rate of tremor occurrence in these segments is not constant over time and the cyclical high and low rates of tremor occurrence may indicate cycles of stress accumulation and release over time.

6.5 On model assumptions

The first assumption that we made for the observed component is using a Bernoulli variable to model the presence/absence of events with a constant p_i over time for the proportion of tremor occurrences each state i. This enabled us to study the difference between the expected proportion of tremor occurrences from the model and the observed tremor occurrences. The significant increasing proportion of tremors compared to the expected proportion before 2003 in segments 1 and 2 and before 2010 in segment 2 in Shikoku (Figure 14) are most likely related to the long-term slow slip events near these segments in 2003 and 2010 [*Obara et al.*, 2010; *Obara*, 2011]. Nevertheless, this assumption may cause tremor events that are located at similar locations but occur in different time periods with significantly different probabilities of tremor occurrences to be classified into different segments. Our next step is to design a model with cyclic temporal variation in the proportion of tremor occurrence. After estimating this cyclic function and obtaining more data for slow slip events with higher temporal resolution, we can then quantify the relationship between tremor and long-term slow slip systematically.

A certain amount of information is lost when only using whether or not there is tremor occurrence in each hour. *Annoura et al.* [2016] identified transient accelerations of total tremor energy released in western Shikoku in 2010 and 2014 during long-term slow slip events. In future research, we should consider adding the energy released by the tremor clusters in each hour into this HMM. By incorporating tremor energy in the model, we can capture the spatiotemporal variation of the intensity of tremor. This can then provide more effective precursory information for short-term slow slip events in terms of both the rate (proportion of tremor occurrence in each segment) and intensity (energy released per hour in each segment) of tremors.

The second assumption for the observed component is that conditioning on presence of tremor, the locations of tremor activity in each segment follow a bivariate

normal distribution. We can then estimate the center and spread of each segment, and thus the final classification of the tremor locations. When applying to tremor data in other areas, if the tremor locations in each segment display obvious skewness, a skewed distribution can be used to classify the locations.

For the hidden component, we assumed a stationary first-order Markov chain for the temporal migration of the distinct spatial segments. This model assumes constant transition probabilities over time and implies a geometric distribution for the sojourn times in each state. The sojourn times in each state in each region in our study appear to follow a geometric distribution. If there is strong evidence suggesting non-stationarity, new models need to be developed to accommodate that, as a stationary model may cause misclassification of some tremor events.

Lastly, we used BIC to select the number of segments in each region. BIC may be conservative and select models with smaller number of states. Model selection for HMMs is an important but still developing area of research. We will investigate this further in the future. If BIC is conservative, then some of the spatiotemporal segments in the two regions may be further divided and their properties can be studied individually. The estimated sojourn times in each segment may also vary.

7 Conclusion

We objectively analyzed the spatiotemporal patterns of the tremor activity in the Kii and Shikoku regions in Japan using an automated method. The tremor activity in these two regions shows a hierarchical structure, characterized by several subsystems each consisting of a group of distinct segments. Each segment in space has unique quantifiable features such as sojourn time, probability of tremor occurrence, and type of tremor.

Tremors can be classified into three types based on their occurrence pattern: episodic, weak concentration, and background. Episodic segments have high tremor activity with a probability of tremor occurrence greater than 0.1 and last for more than four hours on average for the Kii region and more than three hours on average for the Shikoku region. Weak concentration segments feature either low tremor activity with a probability of tremor occurrence less than 0.1 or very short average sojourn times, less than four hours for the Kii region and less than three hours for the Shikoku region. Background states either cover a large geographical region or have very long average sojourn times, more than two days on average for the two regions. For both Kii and Shikoku regions, the average length of the time interval between two active periods of each segment increases with the probabilities of tremor occurrence in the segment.

By comparing the temporal variation of the three types of tremor with the time periods during which short-term slow slip events were detected [*Sekine et al.*, 2010], we concluded that tremor from weak concentration segments often preceded or followed short-term slow slip events, but rarely occurred during the time period of slow slip. This observation provides us a good basis to design a forecasting strategy in the future for short-term slow slip events. When more short-term slow slip events in the two regions with higher temporal resolution are obtained by combining information from both geodetic and seismic data, the transition patterns among the three types of tremor followed by and that not followed by short-term slow slip events can be summarized. These can be used to extract the most likely precursory patterns for short-term slow slip events.

The designed 2D HMM demonstrates its power in analyzing the spatiotemporal occurrence patterns of non-volcanic tremors. It replaces laborious manual analysis of tremor data, enables more effective categorization than was previously possible, and assists us to recognize the most probable classification of the spatial locations in time.

It is automated and provides objective divisions of tremor segments. Moreover, it can be used to produce probabilistic forecasts of future tremor activity, with the forecasting performance evaluated by standard and rigorous statistical procedures.

Acknowledgments

We would like to express our gratitude to the editor Martha Savage, Associate Editor, and two anonymous reviewers for their constructive comments and detailed suggestions that have greatly improved this manuscript. Ting Wang and Jiancang Zhuang are supported by the Marsden Fund administered by the Royal Society of New Zealand. Jiancang Zhuang is also partially supported by the KAKENHI Grant of Japan Society for the Promotion Science, Number 17H00727. This research was supported by JSPS KAKENHI Grant Number JP16H06472 in Scientific Research on Innovative Areas "Science of Slow Earthquakes". We would like to thank Akiko Takeo for helpful discussions and Peter Maxwell and the New Zealand eScience Infrastructure (NeSI) for providing help and access to the PAN Cluster for a major part of computations carried out for the data analysis in this project. The R package "HMMextra0s" that we developed for the HMM in this paper is in the supplementary information. The original hourly tremor catalog is provided from NIED Hi-net web pages, `http://www.hinet.bosai.go.jp/`. NIED hourly tremor catalog can be found in the repository for slow earthquake database `http://www-solid.eps.s.u-tokyo.ac.jp/~sloweq/`. The waveform data for the tremor catalog are provided from NIED Hi-net web pages.

Appendix A: The EM Algorithm

Given the observed data $\mathbf{X}$ and $\mathbf{Z}$, the likelihood of the HMM is

$$\begin{aligned} L(\theta) &= \sum_{s_1,\cdots,s_T=1}^{m} P(\mathbf{X}_1,\cdots,\mathbf{X}_T; Z_1,\cdots,Z_T; S_1=s_1,\cdots,S_T=s_T|\theta) \\ &= \sum_{s_1,\cdots,s_T=1}^{m} P(\mathbf{X}_1, Z_1 \,|\, S_1=s_1,\theta) P(S_1=s_1\,|\,\theta) \\ &\quad \cdot \prod_{t=2}^{T} P(\mathbf{X}_t, Z_t \,|\, S_t=s_t,\theta) P(S_t=s_t \,|\, S_{t-1}=s_{t-1},\theta) \end{aligned} \tag{2}$$

where θ is the set of parameters. As the states of the Markov chain is not observable, we can use the Expectation-Maximization (EM) algorithm [*Baum et al.*, 1970; *Dempster et al.*, 1977] to estimate the parameters by treating the hidden states as missing data. To do this, we first need to write down the complete log likelihood function of this HMM, which is

$$\begin{aligned} \ell^C(\theta,\mathbf{X},\mathbf{Z},\mathbf{S}) &= \sum_{j=1}^{m} I(S_1=j)\log P(S_1=j) + \sum_{t=1}^{T}\sum_{j=1}^{m} I(S_t=j)\log f(\mathbf{x}_t,z_t|S_t=j,\theta) \\ &\quad + \sum_{t=2}^{T}\sum_{i,j=1}^{m} I(S_{t-1}=i,S_t=j)\log P(S_t=j|S_{t-1}=i,\theta) \end{aligned} \tag{3}$$

Set the transition probability from state i to j as $P(S_t=j|S_{t-1}=i)=\gamma_{ij}$, and the initial distribution vector of the Markov chain as $\delta=(\delta_1,\cdots,\delta_m)$. If θ_0 is an initial guess of the parameters, and if we let

$$v_t(j) = P(S_t=j|\mathbf{X}_1,\cdots,\mathbf{X}_T; Z_1,\cdots,Z_T;\theta_0), \tag{4}$$

$$w_t(i,j) = P(S_{t-1}=i,S_t=j|\mathbf{X}_1,\cdots,\mathbf{X}_T; Z_1,\cdots,Z_T;\theta_0), \tag{5}$$

then the E-step is to calculate the expected complete log likelihood

$$\begin{aligned} Q(\theta;\theta_0) &= E_{\mathbf{S},\theta_0}[\ell^C(\theta,\mathbf{X},\mathbf{Z},\mathbf{S})|\mathbf{X},\mathbf{Z}] \\ &= \sum_{j=1}^{m} v_1(j)\log\delta_j + \sum_{t=1}^{T}\sum_{j=1}^{m} v_t(j)\log f(\mathbf{x}_t,z_t|S_t=j,\theta) \\ &\quad + \sum_{t=2}^{T}\sum_{i,j=1}^{m} w_t(i,j)\log\gamma_{ij}. \end{aligned} \tag{6}$$

The M-step is to maximize (6), and the values of the parameters correspond to the maximum of (6) are the parameter estimates.

The likelihood and complete likelihood can be calculated by using the forward and backward probabilities, which are defined recursively as

$$\begin{aligned} \alpha_1(i) &= P(\mathbf{X}_1,Z_1,S_1=i|\theta) = \delta_i f(\mathbf{x}_1,z_1|S_1=i), \\ \alpha_{t+1}(i) &= P(\mathbf{X}_1,\cdots,\mathbf{X}_{t+1},Z_1,\cdots,Z_{t+1},S_{t+1}=i|\theta) \qquad (7) \\ &= \sum_{k=1}^{m}\alpha_t(k)\gamma_{ki}f(\mathbf{x}_{t+1},z_{t+1}|S_{t+1}=j), \qquad (8) \end{aligned}$$

and

$$\begin{aligned} \beta_T(i) &= 1, \\ \beta_t(i) &= P(\mathbf{X}_{t+1},\cdots,\mathbf{X}_T,Z_{t+1},\cdots,Z_T|S_t=i,\theta) \\ &= \sum_{k=1}^{m}\beta_{t+1}(k)\gamma_{ik}f(\mathbf{x}_{t+1},z_{t+1}|S_{t+1}=k). \end{aligned}$$

The likelihood of the HMM in (2) is then

$$L(\theta) = \sum_{i=1}^{m}\alpha_t(i)\beta_t(i). \tag{9}$$

The quantities $v_t(j)$ and $w_t(i,j)$ in the expected complete log likelihood (6) can be computed using

$$\begin{aligned} v_t(j) &= \frac{\alpha_t(j)\beta_t(j)}{\sum_{i=1}^{m}\alpha_t(i)\beta_t(i)}, \\ w_t(i,j) &= \frac{\alpha_{t-1}(i)\gamma_{ij}f(\mathbf{x}_t,z_t|S_t=j)\beta_t(j)}{\sum_{k=1}^{m}\alpha_t(k)\beta_t(k)}. \end{aligned}$$

The M-step is then to maximize the following two terms individually to estimate the parameters

$$\begin{aligned} Q_1(\theta|\theta_0) &= \sum_{t=2}^{T}\sum_{i,j} w_t(i,j)\log\gamma_{ij} \\ Q_2(\theta|\theta_0) &= \sum_{t=1}^{T}\sum_{j=1}^{m} v_t(j)\log f(\mathbf{x}_t,z_t|S_t=j,\theta) \\ &= \sum_{t=1}^{T}\sum_{j=1}^{m} v_t(j)\log\left\{(1-p_j)^{1-z_t}\left[\frac{p_j\exp\left(-(\mathbf{x}_t-\boldsymbol{\mu}_j)^T\boldsymbol{\Sigma}_j^{-1}(\mathbf{x}_t-\boldsymbol{\mu}_j)/2\right)}{2\pi|\boldsymbol{\Sigma}_j|^{1/2}}\right]^{z_t}\right\}, \end{aligned}$$

which gives us the parameter estimates for γ_{ij},

$$\hat{\gamma}_{ij} = \frac{\sum_{t=2}^{T} w_t(i,j)}{\sum_{j=1}^{m}\sum_{t=2}^{T} w_t(i,j)},$$

and for the parameters in the observed process,

$$\hat{p}_j = \frac{\sum_{t=1}^{T} v_t(j) z_t}{\sum_{t=1}^{T} v_t(j)}, \tag{10}$$

$$\hat{\boldsymbol{\mu}}_j = \frac{\sum_{t=1}^{T} v_t(j) z_t \mathbf{x}_t}{\sum_{t=1}^{T} v_t(j) z_t}, \tag{11}$$

$$\hat{\boldsymbol{\Sigma}}_j = \frac{\sum_{t=1}^{T} v_t(j) z_t (\mathbf{x}_t - \hat{\boldsymbol{\mu}}_j)(\mathbf{x}_t - \hat{\boldsymbol{\mu}}_j)^T}{\sum_{t=1}^{T} v_t(j) z_t}. \tag{12}$$

Appendix B: Forecasting algorithm

We assess probabilistic forecasts using the best model with m states for each region. We aim to forecast tremor occurrence and their location at time t given the history of the system until time $t-1$. We use the forward probabilities at time $t-1$

$$\alpha_{t-1}(i) = P(\mathbf{X}_1, \cdots, \mathbf{X}_{t-1}; Z_1, \cdots, Z_{t-1}; S_{t-1} = i)$$

as calculated in the EM algorithm, Equation 7 in the appendix, to forecast the probability that the Markov chain will be in state j at time t, which is

$$\begin{aligned} & P(S_t = j | \mathbf{X}_1, \cdots, \mathbf{X}_{t-1}; Z_1, \cdots, Z_{t-1}) \\ = & \frac{\sum_{i=1}^{m} P(\mathbf{X}_1, \cdots, \mathbf{X}_{t-1}; Z_1, \cdots, Z_{t-1}; S_{t-1} = i) P(S_t = j | S_{t-1} = i)}{\sum_{i=1}^{m} P(\mathbf{X}_1, \cdots, \mathbf{X}_{t-1}; Z_1, \cdots, Z_{t-1}; S_{t-1} = i)} \\ = & \frac{\sum_{i=1}^{m} \alpha_{t-1}(i) \gamma_{ij}}{\sum_{i=1}^{m} \alpha_{t-1}(i)}. \end{aligned}$$

The probability density of a tremor occurring at location $\mathbf{x}$ at time t can be forecast using

$$\sum_{i=1}^{m} P(S_t = j | \mathbf{X}_1, \cdots, \mathbf{X}_{t-1}; Z_1, \cdots, Z_{t-1}) \hat{p}_i \hat{f}(\mathbf{x} \mid z_t = 1, S_t = i),$$

where $\hat{f}(\mathbf{x} \mid z_t = 1, S_t = i)$ is the estimated probability density of tremor location by using the parameters estimated from the data. To visualize the forecast probability density for a period of time and to compare that with the actual observed tremor locations, we can plot the marginal probability density over a specified area in space and a period of time.

References

Annoura, S., K. Obara, T. Maeda (2016), Total energy of deep low-frequency tremor in the Nankai subduction zone, southwest Japan, *Geophysical Research Letters*, *43*, 2562–2567.

Baum, L. E., T. Petrie, G. Soules, and N. Weiss (1970), A maximization technique occurring in the statistical analysis of probabilistic functions of Markov chains, *The Annals of Mathematical Statistics*, *41*, 164–171.

Bebbington, M. S. (2007), Identifying volcanic regimes using hidden Markov models, *Geophysical Journal International*, *171*, 921–942.

Boyarko, D., M. Brudzinski, R. Porritt, R. Allen, and A. Tréhu (2015), Automated detection and location of tectonic tremor along the entire Cascadia margin from 2005 to 2011, *Earth and Planetary Science Letters*, *430*, 160–170.

Brudzinski, M. R., and R. M. Allen (2007), Segmentation in episodic tremor and slip all along Cascadia, *Geology*, *35*, B06,302.

Dempster, A. P., N. M. Laird, and D. B. Bubin (1977), Maximum likelihood from incomplete data via EM algorithm (with discussions), *Journal of Royal Statistical Society, Series B*, *39*, 1–38.

Forney, G. D. (1973), The Viterbi algorithm, *Proceedings of the IEEE*, *61*, 268–278.

Granat, R. A., and A. Donnellan (2002), A hidden Markov model based tool for geophysical data exploration, *Pure and Applied Geophysics*, *159*, 2271–2283.

Hirose, H., and K. Obara (2005), Repeating short- and long-term slow slip events with deep tremor activity around the Bungo channel region, southwest Japan, *Earth Planets Space*, *57*, 961–972.

Hirose, H., and K. Obara (2010), Recurrence behavior of short-term slow slip and correlated non-volcanic tremor episodes in western Shikoku, southwest Japan, *Journal of Geophysical Research*, *115*, B00A21.

Hirose, H., Y. Asano, K. Obara, T. Kimura, T. Matsuzawa, S. Tanaka, and T. Maeda (2010), Slow earthquakes linked along dip in the Nankai subduction zone, *Science*, *330*, 1502.

Holtkamp, S., and M. R. Brudzinski (2010), Determination of slow slip episodes and strain accumulation along the Cascadia margin, *Journal of Geophysical Research*, *115*, B00A17.

Ide, S. (2010), Striations, duration, migration and tidal response in deep tremor, *Nature*, *466*, 356–360.

Kao, H., and S.-J. Shan (2004), The source-scanning algorithm: Mapping the distribution of seismic sources in time and space, *Geophysical Journal International*, *157*, 589–594.

MacDonald, I., and W. Zucchini (1997), The seismic cycle, quantitative seismic zoning, and long-term seismic forecasting, in *Hidden-Markov and Other Models for Discrete valued Time Series*, Chapman & Hall, New York.

Maeda, T., and K. Obara (2009), Spatiotemporal distribution of seismic energy radiation from low-frequency tremor in western Shikoku, Japan, *Journal of Geophysical Research*, *114*, B00A09.

Obara, K. (2002), Nonvolcanic deep tremor associated with subduction in southwest Japan, *Science*, *296*, 1679–1681.

Obara, K. (2010), Phenomenology of deep slow earthquake family in southwest Japan: spatiotemporal characteristics and segmentation, *Journal of Geophysical Research*, *115*, B00A25.

Obara, K. (2011), Characteristics and interactions between non-volcanic tremor and related slow earthquakes in the Nankai subduction zone, southwest Japan, *Journal of Geodynamics*, *52*, 229–248.

Obara, K., and A. Kato (2016), Connecting slow earthquakes to huge earthquakes, *Science*, *353 (6296)*, 253–257.

Obara, K., H. Hirose, F. Yamamizu, and K. Kasahara (2004), Episodic slow slip events accompanied by non-volcanic tremors in southwest Japan subduction zone, *Geophysical Research Letters*, *31*, L23,602.

Obara, K., S. Tanaka, T. Maeda, and T. Matsuzawa (2010), Depth-dependent activity of non-volcanic tremor in southwest Japan, *Geophysical Research Letters*, *37*, L13,306.

Obara, K., T. Matsuzawa, S. Tanaka, T. Kimura, and M. T. (2011), Migration properties of non-volcanic tremor in Shikoku, southwest Japan, *Geophysical Research Letters*, *38*, L09,311.

Obara, K., T. Matsuzawa, S. Tanaka, and T. Maeda (2012), Depth-dependent mode of tremor migration beneath Kii Peninsula, Nankai subduction zone, *Geophysical Research Letters*, *39*, L10,308.

Orfanogiannaki, K., D. Karlis, and G. A. Papadopoulos (2010), Identifying seismicity levels via Poisson hidden Markov models, *Pure and Applied Geophysics*, *167*, 919–931.

Ozawa, S., Y. Hatanaka, M. Kaidzu, M. Murakami, T. Imakiire, and Y. Ishigaki (2004), Aseismic slip and low-frequency earthquakes in the Bungo channel, southwestern Japan, *Geophysical Research Letters*, *31*, L07,609.

Peterson, C. L., and D. H. Christensen (2009), Possible relationship between nonvolcanic tremor and the 1998–2001 slow slip event, south central Alaska, *Journal of Geophysical Research*, *114*, B06,302.

Rogers, G., and H. Dragert (2003), Episodic tremor and slip on the Cascadia subduction zone: the chatter of silent slip, *Science*, *300*, 1942–1943.

Schwarz, G. (1978), Estimating the dimension of a model, *Annals of Statistics*, *6*, 461–464.

Sekine, S., H. Hirose, and K. Obara (2010), Along-strike variations in short-term slow slip events in the southwest Japan subduction zone, *Journal of Geophysical Research*, *115*, B00A27.

Shelly, D. R., G. C. Beroza, S. Ide, and N. S. (2006), Low-frequency earthquakes in Shikoku, Japan and their relationship to episodic tremor and slip, *Nature*, *442*, 188–191.

Viterbi, A. J. (1967), Error bounds for convolutional codes and an asymptotically optimum decoding algorithm, *IEEE Transactions on Information Theory*, *IT-13*, 260–269.

Wang, T., and M. S. Bebbington (2013), Identifying anomalous signals in GPS data using HMMs: An increased likelihood of earthquakes?, *Computational Statistics and Data Analysis*, *58*, 27–44.

Wang, T., M. S. Bebbington, and D. S. Harte (2012), Markov-modulated Hawkes process with stepwise decay, *The Annals of the Institute of Statistical Mathematics*, *64*, 521–544.

Wang, T., J. Zhuang, K. Obara, and H. Tsuruoka (2016), Hidden Markov modeling of sparse time series from non-volcanic tremor observations, *Journal of the Royal Statistical Society, Series C, Applied Statistics*, doi:10.1111/rssc.12194.

Wech, A. G., and K. C. Creager (2011), A continuum of stress, strength and slip in the Cascadia subduction zone, *Nature Geoscience*, *4*, 624–628.